In-cylinder measurements of NO formation in a Diesel engine

G.G.M. Stoffels, E.J. van den Boom, C.M.I. Spaanjaars, N. Dam, W.L. Meerts and J.J. ter Meulen

Applied Physics, University of Nijmegen
Toernooiveld, NL-6525ED Nijmegen, The Netherlands

J.L.C. Duff and D.J. Rickeard

Esso Research Centre
Abingdon, Oxon OX13 6AE, UK

ABSTRACT

The formation of Nitric oxide (NO) in a Diesel engine has been studied as a function of crank angle throughout the whole combustion cycle, using the Laser Induced Fluorescence (LIF) technique. Measurements were performed in an optically accessible one-cylinder, two-stroke, direct injection Diesel engine. The engine was operated in steady state at different loads and compression ratios. A tunable ArF excimer laser beam was used to excite the NO molecules in the $D^2\Sigma^+(v'=0) \leftarrow X^2\Pi(v''=1)$ band at 193 nm. Dispersed fluorescence spectra allowed to discriminate between NO and interfering oxygen fluorescence. From the spectra, a relative measure for the NO density present in the probed volume of the cylinder was obtained. This density was transformed into an in-cylinder NO content, taking into account the changes in laser intensity, pressure, temperature and volume during the stroke. The resulting NO content curves show a slow start of the NO formation at the beginning of the combustion, gradually rising to a broad maximum around 50° aTDC. It is concluded that, in this engine, the bulk of NO formation takes place relatively late in the stroke. This suggests that the diffusion burning phase of combustion makes an important contribution to the NO formation, contrary to the model which assumes that NO is formed mainly during the initial premixed burn.

INTRODUCTION

The Diesel engine offers the benefits of high fuel economy and reduced CO_2 emissions. However, compared to gasoline engines, its disadvantage lies in its emissions of nitric oxides (NO_x) and particulate matter (PM), which are meeting increasingly stringent regulations in Europe, North America, and the Far East. The chemistry of NO_x formation is thought to be well understood, but the complex physics of diesel injection and combustion makes an analytical approach to understanding NO formation in a Diesel engine difficult. The objective of this work was to quantify the nitric oxide (NO) content of a Diesel engine cylinder as a function of time throughout the whole combustion cycle using optical diagnostics based on Laser Induced Fluorescence.

Laser-based diagnostics are of interest for the study of combustion processes because they allow non-intrusive, spatially and temporally resolved measurements of specific chemical species [1]. The combination of resonant Mie scattering and Two-Dimensional Laser Induced Incandescence (2D-LII) can be used to visualize in-cylinder soot distributions in Diesel engines [2, 3]. The Laser Induced Fluorescence (LIF) technique has the sensitivity to provide information about the different molecules present in combustion processes. This LIF technique is in principle a two step process: electronic excitation of molecules by a laser beam and detection of the ensuing fluorescence. The fluorescence can be dispersed by a monochromator to obtain spectrally resolved information or a filter can be used to single out a specific fluorescence wavelength. By the use of the Planar LIF (PLIF) technique, which involves excitation by a thin laser sheet and detection of the fluorescence through a filter in a direction perpendicular to the sheet, two-dimensional images can be obtained. The (P)LIF technique has been used to demonstrate the presence of a large variety of molecular species in combustion processes, but quantification of fluorescence signals is difficult. The fluorescence signal is proportional to the local density of molecules excited by the laser beam and to the fraction of excited molecules that fluoresces at the right wavelength. However, the proportionality constant depends strongly on the local pressure and temperature, the local laser intensity and the chemical composition of the environment. Since most of these parameters are not known and difficult to measure, some assumptions have to be made to obtain quantitative data. Another problem is the possible spectroscopic interference between different molecules.

The LIF technique has been applied before to both SI engines (see e.g. the recent work of Sick *et al.* [4, 5] and references in there) and to Diesel engines [6, 7, 8, 9] to mea-

sure the in-cylinder NO distribution and the in-cylinder NO content. Nakagawa *et al.* [7] applied PLIF imaging to a single fuel jet Diesel research engine running on a mixed fuel to minimize soot production. However, to obtain sufficient NO fluorescence they used oxygen enriched intake air. Their results showed the location of the NO relative to the reacting fuel jet, but the start and the end of the NO formation are not determined. They did not correct their data for changes in laser intensity, pressure, temperature and mixing to obtain some quantitative information about the amount of NO present in the cylinder.

Recently, an impressive paper by Dec and Canaan [8] presented NO distributions showing the timing and location of NO formation in a DI Diesel engine running on a low-sooting fuel, obtained by single-shot PLIF imaging. They used a tripled Nd:YAG laser pumping a narrow-line optical parametric oscillator (OPO) to excite the NO molecules in the $A(v'=0) \leftarrow X(v''=0)$ band at 226.035 nm and detected the fluorescence of the $A(v'=0) \rightarrow X(v''=1,2,3,4)$ bands. In addition to the NO distributions, a curve of the total averaged NO PLIF intensity as a function of crank angle was shown, obtained by integrating the NO PLIF signal over a representative sector of the combustion chamber. In order to determine the total in-cylinder NO content the integrated NO PLIF signal was corrected for the effects of pressure, temperature and mixing. However, no attention was given to the attenuation of the laser intensity or the induced fluorescence on its way through the combustion chamber. They found that NO formation does not start during the premixed combustion (which is fuel rich), but begins around the fuel jet periphery just after the diffusion flame forms, where it remains until the jet structure begins to disappear. As the burn-out phase continues, NO remains along the track of the fuel jet, and the NO formation continues in the hot post-combustion gases after the end of combustion. The NO content curve shows that only 67% of the NO has formed by the end of the apparent heat release, so NO formation must continue in the post-combustion gases after the diffusion flame has gone out.

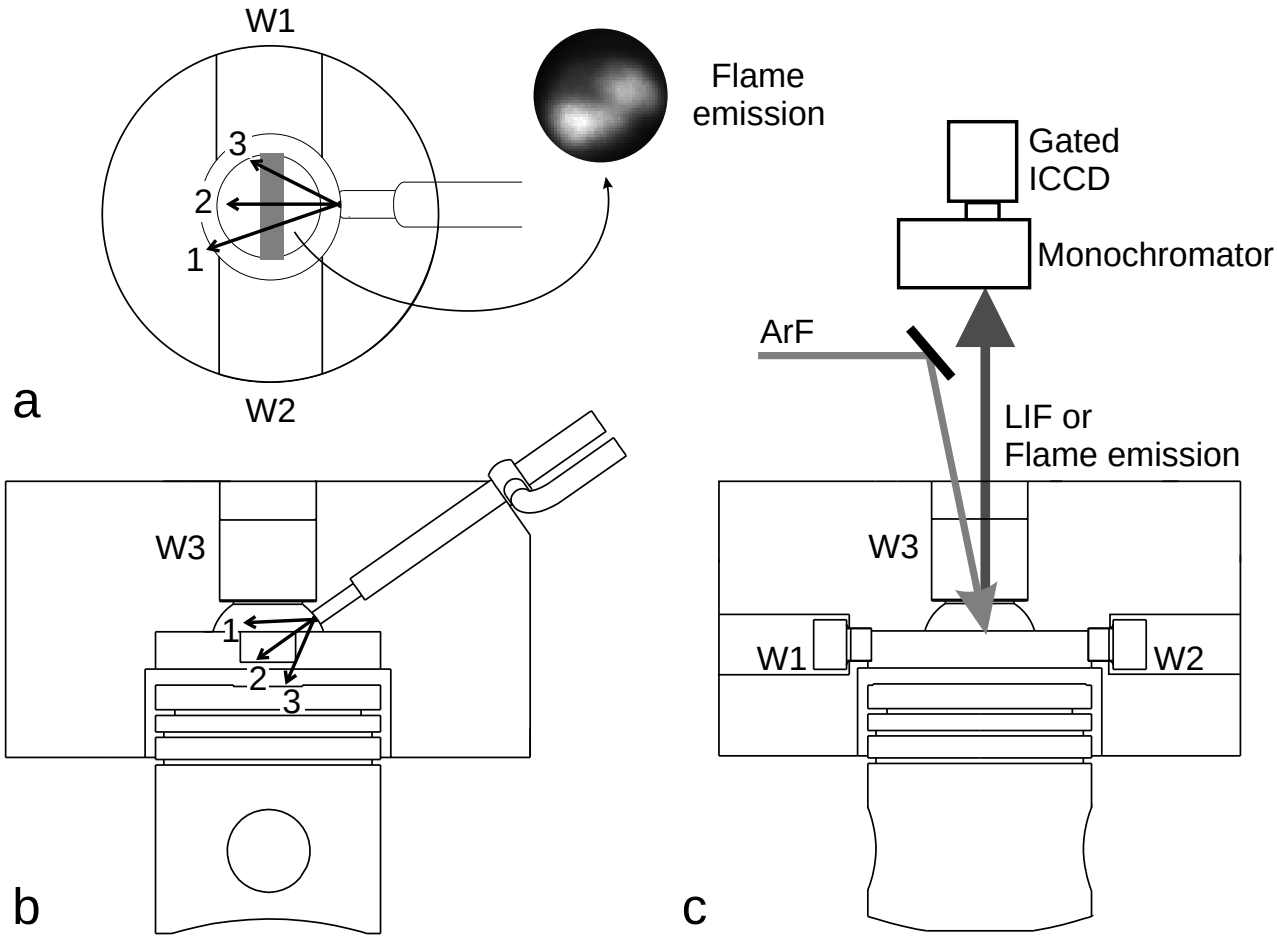

Figure 1: Schematical view of the modified two-stroke Diesel engine and the optical setup. The engine is optically accessible by two windows in the side wall (side windows; W1,2) and the window in the top of the cylinder head (top window; W3). The ArF excimer laser beam enters the combustion chamber through the top window. The induced fluorescence or natural flame luminosity is detected through the top window by a gated CCD camera, positioned behind a monochromator. Spray directions of the three-hole nozzle are indicated (arrows 1–3 in a) and b)); an image of the natural flame luminosity (recorded at TDC) is shown in the insert to figure a).

Engine Make	Sachs
Engine Type	Two-stroke, One-cylinder, DI Diesel
Bore	81.5 mm
Stroke (effective)	80 mm (55 mm)
Cylinder capacity	412 cc
Fuel injection	direct, 3 hole injector
Exhaust port opening	105° aTDC
Intake port opening	121° aTDC

Table 1: Specifications of the modified engine.

Engine speed	1200 rpm
Injection timing	27° bTDC
Intake air pressure	1.2 bar (absolute)
Intake air temperature	320 K (estimated)
Compression ratio	12.4, 13.4, 14.4
Load	0.44, 0.75, 0.88 kW
Fuel	Diesel fuel (2 types, numbered 1 and 2)
	Production Diesel (see table 3)

Table 2: Operating conditions of the modified engine.

In the present work, the LIF technique was used to obtain dispersed fluorescence spectra of NO from an optically accessible two-stroke DI Diesel engine. The engine was operated in normal mode (i.e. not skip-fired) on standard production Diesel fuel and ambient (non-oxygen-enriched) intake air. Using an excimer laser to excite the NO molecules in the $D(v='0) \leftarrow X(v''=1)$ band at 193.377 nm, NO fluorescence could be detected during the whole combustion process. Dispersed fluorescence spectra in the wavelength range between 200 nm and 230 nm were obtained as a function of crank angle using a monochromator. The main advantage of dispersed fluorescence spectra over images is that the spectra allow discrimination between NO and Oxygen (O_2) fluorescence. When the fluorescence was dispersed into its different wavelength components the interference of NO and O_2 fluorescence could clearly be seen. The spectra allowed to discriminate against O_2 fluorescence and to arrive at a semi-quantitative measure for the amount of NO inside the probed volume of the cylinder as a function of crank angle. These data were processed for the changes in laser intensity, pressure, temperature and volume during the stroke in order to obtain an in-cylinder NO density as a function of crank angle.

A second aim of this work was also to make a qualitative/quantitative assessment of the effect on NO production of engine conditions (compression ratio and load) and fuel. To that end, dispersed fluorescence spectra of NO were measured for different engine conditions and fuels.

This paper begins with a description of the experimental method, including the engine, its operating conditions and the optics used to obtain the dispersed fluorescence spectra. Then the results are presented: the engine characteristics observed, the fluorescence spectra obtained by dispersing the LIF signal, and the translation of the fluorescence yield into a semi-quantitative measure of NO content. These results are then discussed in terms of the effects of engine conditions and fuels on NO formation. Finally, the findings of this work are compared with current theoretical and experimental measurements of NO in the literature and some conclusions are drawn.

EXPERIMENTAL METHOD

ENGINE

Measurements were performed on a one-cylinder, direct-injection (DI), two-stroke Diesel engine. The engine was modified quite considerably, as described below, in order to provide full optical access during the whole cycle. As a result, it may not be very representative for typical production engines, but is well suited for the evaluation of laser diagnostics, one of the aims of the present work. The modified engine is shown schematically in figure 1 and its specifications are given in table 1. The combustion chamber of the engine was made optically accessible by mounting two quartz (Suprasil I) windows in the cylinder wall (side windows (W1,2 in fig. 1); 25 × 10 mm, thickness 25 mm) and one in the top of the cylinder head (top window (W3); diameter 25 mm, thickness 35 mm). A piston with a slot of 0.5 mm depth and a width of 25 mm in its upper surface was used to provide optical access through the side windows during the whole combustion stroke. As the top window was placed at the original position of the injector, fuel was injected through a modified three hole injector placed at an angle of 55 degrees with the cylinder axis, as shown in figure 1b. The three sprays (35° angle between them) all lay in one plane containing the injector axis. In order to prevent one of the sprays hitting the laser beam entrance window (W1), the spray plane was rotated 30° around the injector axis. Fuel injection starts at 27° bTDC with an (initial) injection pressure of 170 bar. The original scavenging ports and inlet were closed, in or-

Fuel Code	Fuel 1	Fuel 2
Density (g/ml)	0.8242	0.8233
Distillation (°C)		
IBP	166	184
T10	194	215
T50	235	250
T90	326	292
T95	347	309
FBP	364	327
Sulphur (%m/m)	0.16	0.02
Cetane Number	47.1	53.2
Aromatics HPLC (%m/m)		
1-ring	15.1	14.0
2-ring	2.9	2.6
3-ring	0.7	0.2
Total	18.7	16.8
Viscosity (cSt at 40°C)	2.04	2.25

Table 3: Details of the test fuels.

der to avoid particulates to flow from the crank case to the measurement volume where they could strongly attenuate the laser beam. The fresh air required for the combustion was added through a new inlet at a small overpressure (0.2 bar) in order to improve scavenging. Because conventional oil is not UV transparent, an alternative, chemically inert, UV transparent oil (Fomblin Y25, Ausimont S.P.A.) was used in order to avoid attenuation of the laser beam by the oil film that is formed on the windows. Since, however, the lubricating qualities of this oil are poor, operating times were limited to about 20 minutes, and the engine could only be operated at low load. Window fouling turned out to be relatively unimportant. The top window (W3) stayed clear during the whole measurement period (although it became slightly etched in the long run). The engine was operated in steady-state at 1200 rpm on different fuels and compression ratios and loaded by an electric water-cooled brake at various loads. Operating conditions are summarized in table 2. Note that, as a result of all modifications, the compression ratio of this engine is relatively low.

DETAILS OF TEST FUELS

The two fuels selected were standard production automotive diesel oil, meeting the European EN590 specification. The details of the test fuels are given in table 3. The main differences between them were that fuel 2 had a narrower distillation range, lower T95, lower sulphur content, and higher cetane number than fuel 1.

OPTICAL SETUP

The optical setup used in the LIF experiments is also indicated schematically in figure 1. A pulsed ArF excimer laser (Λ-Physik, Compex 350T), tunable between 192.9 and 193.9 nm with 20 ns pulse duration and a bandwidth of 1 cm^{-1}, was used to excite nitric oxide molecules at the $R_1(26.5)/Q_1(32.5)$ transition in the $D^2\Sigma^+(v'=0) \leftarrow X^2\Pi(v''=1)$ band at 193.38 nm [10]. This transition was selected to minimize interference from vibrationally hot oxygen, that has several strong absorptions within the tuning range of the excimer laser [11, 12, 13, 14]. The laser was synchronised to the position of the piston with an accuracy of 0.6 degree crank angle. It was manually tuned to resonance with the NO transition before each measurement cycle; frequency drift during each measurement was less than the laser bandwidth and negligible with respect to the observed NO line widths. A normal incidence 193 nm laser mirror was used in front of the collection optics to suppress Mie scattered radiation.

To obtain dispersed fluorescence spectra, the unfocused, rectangular laser beam (25×3 mm^2) was coupled into the combustion chamber through the top window, with a pulse energy of 130 mJ, typically. The area illuminated by the laser beam is indicated in figure 1a. The ensuing fluorescence was coupled out also through the top window, and detected by a gated (50 ns) intensified CCD camera (Princeton Instruments, ICCD-576G/RB-E) placed behind a monochromator (Chromex 250i; 1200 gr/mm grating, entrance slit width 50 μm, slit oriented parallel to the length of the illuminated area), which was used to disperse the induced fluorescence in its different wavelength components. This system effectively constitutes an Optical Multichannel Analyzer (OMA). The spectrally resolved fluorescence was averaged over the height of the slit, and therefore represents an average over the whole probe volume.

The main advantage of this setup is that the laser beam enters the combustion chamber directly within the observation area; attenuation losses are therefore kept to a minimum and nearly all laser intensity can be used for excitation of NO. A disadvantage, however, is that part of the spatial resolution is lost, because the combustion chamber is illuminated along the line of sight of the detector. Furthermore, there is a contribution to the scattered signal at 208 nm, the wavelength that is most suitable for recording in-cylinder distributions of NO, that appears to

be due to Raman scattering by the quartz top window. These facts preclude obtaining NO fluorescence distributions by illumination through the top window.

RESULTS AND DISCUSSION

ENGINE CHARACTERISTICS

To obtain some information about the characteristics of the modified engine, the in-cylinder pressure was measured for the different engine operating conditions. This was used, together with the volume, to calculate the heat release and the mean gas temperature, on the assumption of an ideal gas in the cylinder and neglecting crevice flows [16].

A typical in-cylinder pressure curve and its derivative with respect to crank angle are given in figures 2a and b. (Similar curves were obtained at other engine conditions.) In this case the engine was running on Diesel fuel 1, at a compression ratio of 14.4 and loaded by 0.44 kW. In the modified engine the peak pressure, typically around 75 bar, is already reached at Top Dead Centre (TDC). At the moment the exhaust opens the pressure has dropped to 2 bar. The maximum change in pressure as derived from the derivative of the pressure is 7.4 bar/dca[1], which is relatively large. The heat release calculated from the curves of figures 2a and b and the volume is given in figure 2c. The mean gas temperature inside the cylinder is derived from the heat release curve, taking an air temperature of 320 K at the moment the exhaust port closes. This temperature curve is given in figure 2d (solid curve) and shows a maximum temperature of 1470 K a few degrees after TDC, dropping to about 580 K just before the exhaust opens.

Since the mean gas temperature is not necessarily decisive with respect to the NO formation, it is of interest to look at another measure of (local) temperature, as can be obtained from the natural flame luminosity [15]. Combustion was seen to start around 15° bTDC and the natural flame emission, appearing white to the unaided eye, could be observed till around 60° aTDC. The intensity of the observed flame luminosity (integrated over the observation area) is included in figure 2c. Evidently, the visible combustion continues long after the main contribution to the heat release. Dispersing the flame emission results in a spectrum which shows no spectral structure that might be ascribed to fluorescence of excited molecules. This indicates that it results mainly from glowing soot particles. The spectrum can be fitted to a Planck black body radiation curve and can therefore be used to determine a temperature. By recording the dispersed natural flame emission for all different crank angles at which the emission could be observed, a temperature as a function of crank angle is obtained. This so-called soot temperature is also given in figure 2d (solid black squares). The dashed curve is an extrapolation based on adiabatic expansion of an ideal gas (γ=1.36) during the later part of the stroke, matched to the intermediate part of the measured data. This soot temperature has a maximum of about 2300 K and is much higher than the mean gas temperature. The reason for the difference is found in the fact that the cylinder contents are not likely to be in thermal equilibrium. The mean gas temperature represents an average temperature of the gas inside the whole cylinder, whereas the soot temperature represents the temperature of the locally present soot. This latter temperature is obtained from the actual combustion where the temperature is locally high and not yet in equilibrium with the rest of the gas in the cylinder. The high temperature obtained for the soot is in agreement with the temperature following from the colour of the flame emission. The white colour indicates a temperature of carbon particles around 2000 - 2500 K [16].

The shapes of the pressure curve, its derivative and the heat release indicate that the engine conditions were not optimal. However, a compromise had to be found between low engine wear and high NO production. Under normal operating conditions (high load, high speed), the engine wear (liner and rings) would increase dramatically due to the use of the alternative lubricant. In the present experiments the load and the engine speed were kept low and the injection timing was advanced, resulting in a higher peak pressure and temperature. As a result, the NO formation was increased while the soot production was kept low.

DISPERSED FLUORESCENCE SPECTRA

Dispersed fluorescence spectra were obtained by coupling in the laser beam through the top window and detecting the fluorescence also through the top window with the OMA system. The laser induced fluorescence, dispersed into its wavelength components between 200 nm and 230 nm, is shown in figure 3 for different crank angles. During the measurement of this series of dispersion spectra, the engine was running on Diesel fuel 1 at a compression ratio of 14.4 and loaded by 0.44 kW. The spectra are averaged over 100 engine cycles and represent an average fluorescence signal of a narrow strip (25 × ca. 0.5 mm) with a vertical extent depending on the penetration depth of the laser radiation. No background signal from natural flame emission is observed in this wavelength region with the used camera gate width of 50 ns, so that all observed signal is laser induced. The peak at 207.8 nm present in all spectra is an artefact of the measurement setup, caused probably by Raman scattering of the quartz top window. All spectra show spectral structure indicating that fluorescence can be obtained through the whole stroke, even at TDC where the pressure and temperature are high and attenuation of the laser radiation is strong.

Around 30° aTDC, a conspicuous qualitative change in spectral structure and intensity is seen. The grey bands in figure 3 mark the spectrally broad structures at 208 nm (red shoulder of the quartz phosphorescence peak), 216 nm and 225 nm. These structures can be attributed to NO fluorescence from the directly excited D(v′=0)-state to the X(v″=3,4,5)-states, respectively (the D(v′=0) → X(v″=2) band at 201 nm is suppressed by the 193 nm mirror). The two weaker emission signals seen at

[1] dca=degree crank angle

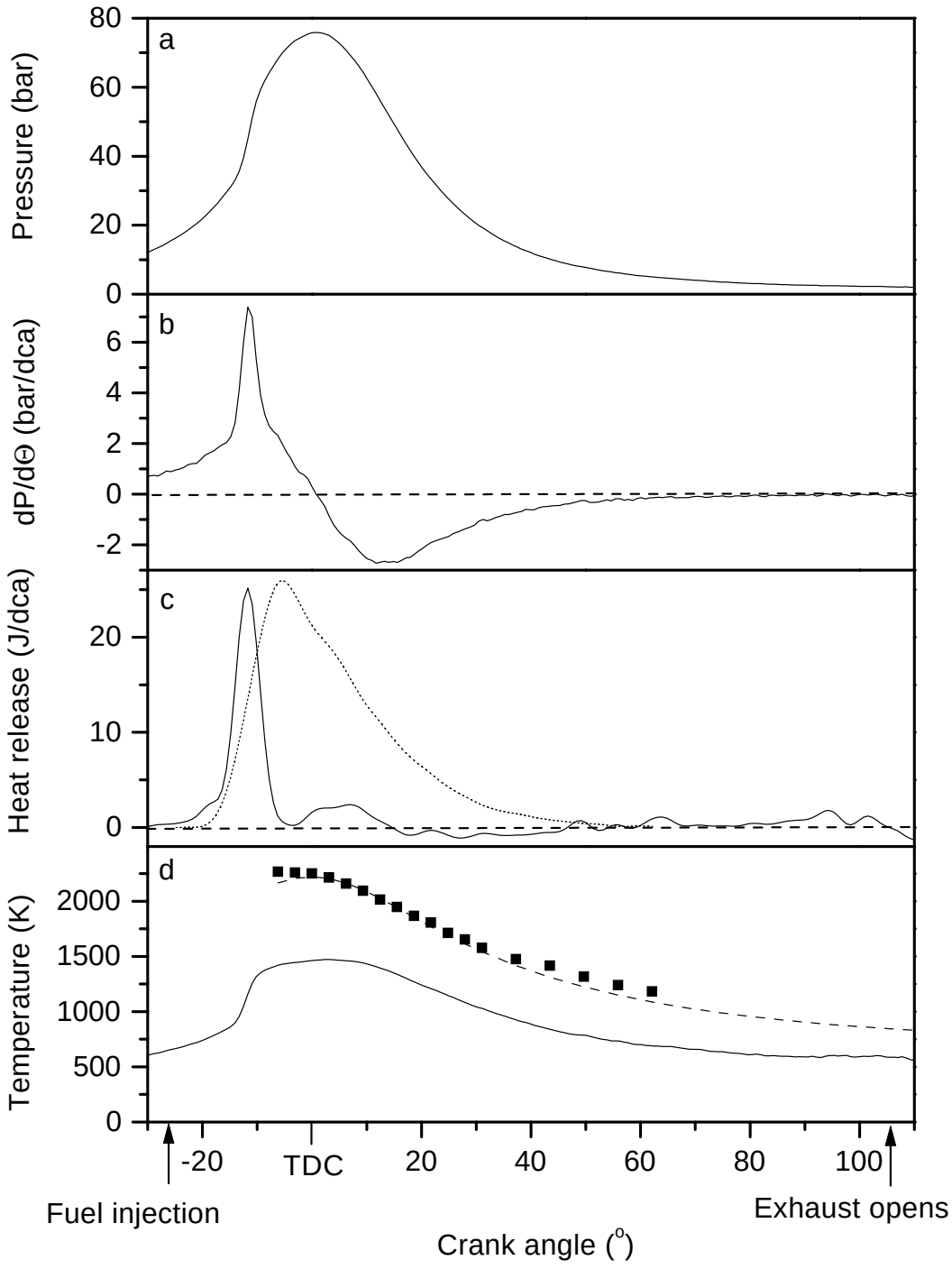

Figure 2: Parameters of the modified Diesel engine running steadily on Diesel fuel 1 at a compression ratio of 14.4 and loaded by 0.44 kW. a) Pressure; b) Derivative of the pressure with respect to crank angle; c) Heat release (solid curve) and integrated intensity of the natural flame emission (dashed curve); d) Mean gas temperature derived from the heat release (solid curve) and soot temperature derived from the spectrum of the natural flame emission (solid black squares). The dashed curve is an extrapolation based on adiabatic expansion of an ideal gas during the later part of the stroke, matched to the intermediate part of the measured data.

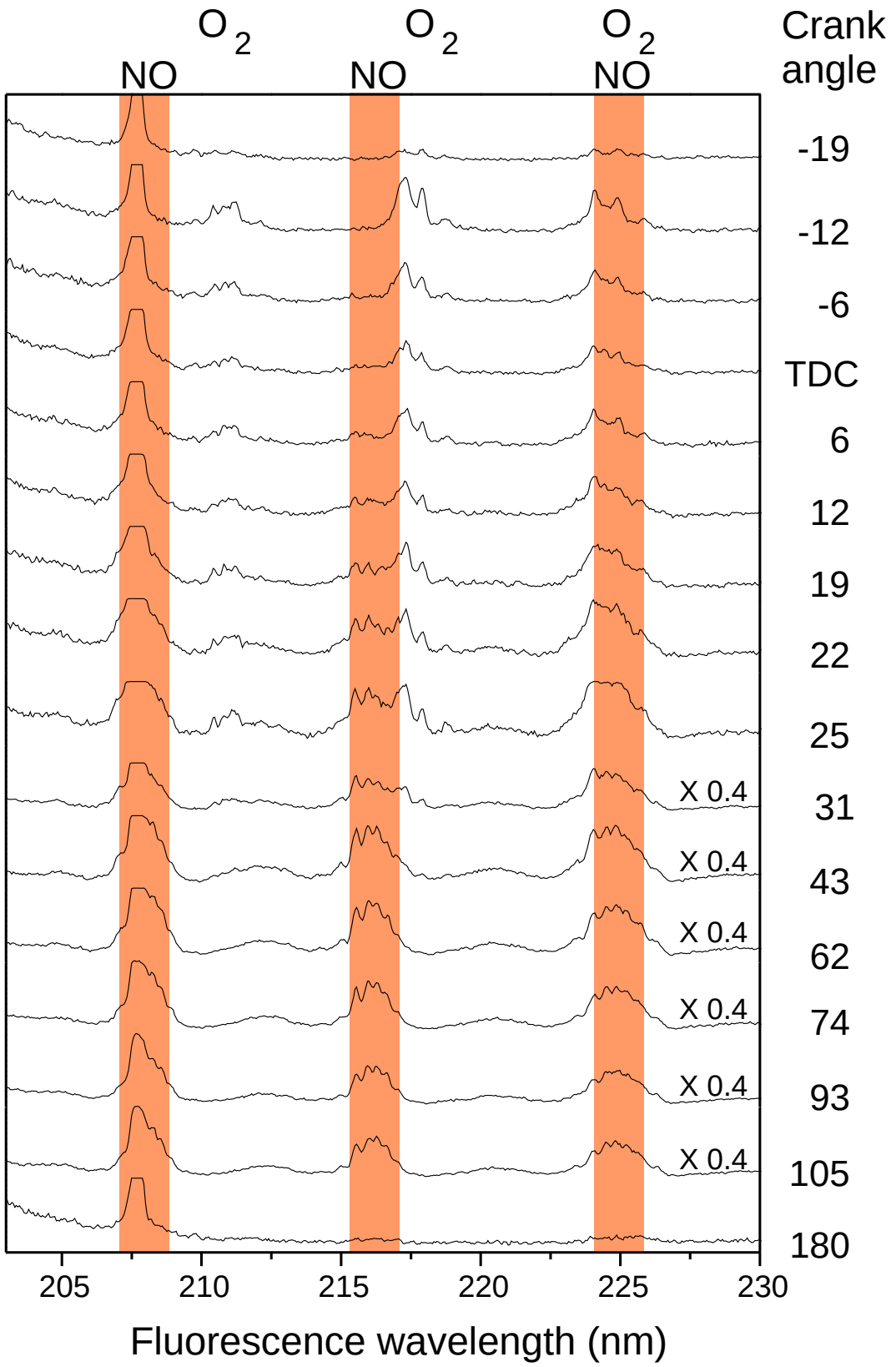

Figure 3: Dispersed fluorescence spectra of NO (averaged over 100 engine cycles) at different crank angles obtained from the engine running on Diesel fuel 1 at a compression ratio of 14.4 and loaded by 0.44 kW. All spectra are at the same scale unless indicated otherwise. The persistent peak at 207.8 nm is an artefact of the quartz top window. The grey bands indicate the positions of the $D^2\Sigma^+(v'=0) \rightarrow X^2\Pi(v''=3,4,5)$ bands of NO.

212.5 nm and 220 nm (for $\Theta \gtrsim 40°$ aTDC) result from NO fluorescence out of the C(v′=0)-state, populated by Electronic Energy Transfer (EET), to the X(v″=3,4)-states. For $\Theta \lesssim 30°$ aTDC, additional peaks at 211 nm and 217.5 nm are present besides the NO signals. These fluorescence features can be ascribed to hot oxygen (O_2). Within the tuning range of an excimer laser operated on ArF a number of O_2 transitions in the Schumann-Runge $B^3\Sigma_u^+ \leftarrow X^3\Sigma_g^-$ system can be excited, the strongest of which start from v″=2 or 3 [11, 12, 13, 14]. At the high temperatures that are reached during the combustion around TDC, these vibrationally excited levels are sufficiently populated to give fluorescence signals. When using an ArF laser, completely avoiding O_2 excitation at high temperatures is difficult because all strong NO transitions lie close to some O_2 resonance. The O_2 fluorescence is characterized by narrow doublet structures, due to fast predissociation of the upper state [11, 12, 13]. Also the doublet structure seen at 225 nm near TDC is the result of fluorescence of O_2. Around 225 nm, only the shape of the peak changes with increasing crank angle from a doublet structure (characteristic for O_2) for $\Theta \lesssim 30°$ aTDC to a broad, rippled structure (characteristic for NO) for $\Theta \gtrsim 30°$ aTDC, because the fluorescence bands of NO and O_2 coincide in this wavelength region. Although NO fluorescence is the most evident in the spectra for $\Theta \gtrsim 30°$ aTDC, it can already be seen in the spectrum recorded at 6° bTDC. The spectrum at 180° aTDC (BDC) shows no NO fluorescence, indicating that every cycle all NO is removed by scavenging. (For comparison, Bräumer *et al.* found that five cycles were needed to completely remove all NO in their SI engine [17]). At 180° aTDC, no oxygen fluorescence is seen neither, because of the small population of the $v'' = 2$ and 3 as a result of the low temperature at that moment.

Similar series of spectra, reproducing well, were obtained for several engine runs. Also, dispersed fluorescence spectra were obtained for other engine conditions. They show the same spectral structures and only little difference is seen in the intensity of the NO fluorescence peaks, mainly around TDC. The NO dispersion spectra provide information on the amount of NO present inside the probed volume of the cylinder, which can be used to obtain an in-cylinder NO density. They also provide information about the wavelengths of the fluorescence bands of NO and O_2 obtained from the running engine. This information is necessary to determine a fluorescence band of NO free from O_2 fluorescence for imaging of NO distributions.

NO DENSITY

The area below the NO fluorescence peaks in the dispersion spectra (the so-called fluorescence yield) provides information on the amount of NO present inside the probed volume of the cylinder at different crank angles. To compare the fluorescence yields at different crank angles and engine conditions it is necessary to convert them into more quantitative data. However, as almost all NO fluorescence bands are overlapped by O_2 fluorescence, the structures due to O_2 fluorescence have to be taken into account. From this point of view the NO fluorescence band at 208 nm would be best suited for evaluation, but unfortunately it is exactly at this wavelength that interference with a signal originating from the quartz window occurs. Alternatively, the NO peak at 216 nm was used, because it is only slightly mixed with the O_2 fluorescence at 217.5 nm. To determine the contribution of O_2, the peaks in the 12° bTDC spectrum (where only O_2 fluorescence is present) are fitted to Gaussian curves. Because the position and shape of the O_2 peaks do not change during the stroke (a benefit of the fast predissociation of the B-state), this result can be used, together with a proportionality constant for the change in intensity, to determine the O_2 contribution to the emission in the 216-218 nm region at all crank angles. Taking this contribution into account, the NO fluorescence at 216 nm is fitted to a Gaussian curve in order to obtain an NO fluorescence yield. Following this procedure, fluorescence yield curves as a function of crank angle are obtained for the engine at different operating conditions (fuel, load, compression ratio). The fluorescence yield curve obtained from the spectra presented in figure 3 is given in figure 4a (open squares). Curves obtained for other engine conditions look rather similar and most of the differences are seen around TDC (discussed below). However, comparison of just the fluorescence yields would be deceptive because they also depend on the pressure, temperature and laser radiation intensity inside the cylinder. These parameters vary during the stroke and for different engine conditions. Therefore, in order to compare the fluorescence yields throughout the stroke and for different engine conditions, they have to be translated into an in-cylinder NO concentration, taking into account the changing in-cylinder conditions. The model used to process the measured fluorescence yield is described in the Appendix.

Two NO density curves as a function of crank angle derived from the fluorescence yield curve in figure 4a following the procedure described in the Appendix, are given in figure 4b. The difference between the curves is the temperature used in the processing. The curve with solid black squares results from using the mean gas temperature whereas the curve with solid circles results from using the soot temperature. For comparison these two temperature curves are included in figure 4a. For both curves the in-cylinder pressure given in figure 2 is used. Under the assumption that the probe volume is representative for the whole cylinder content (see Appendix and figure 1c), NO content curves can be derived from the density curves, resulting in figure 4c.

Before discussing the shape of the curves in figure 4, some discussion concerning possible error sources is appropriate. However, since most of these are systematic errors that appear in all NO content curves they do not affect the relative differences between curves, and NO content curves at different engine conditions can be compared. Because the fluorescence yield curves obtained for several engine runs reproduce well, the accuracy of the obtained NO content curve will be determined mainly by the precision of the fluorescence yield processing method. Although the general relationship between the fluorescence yield and

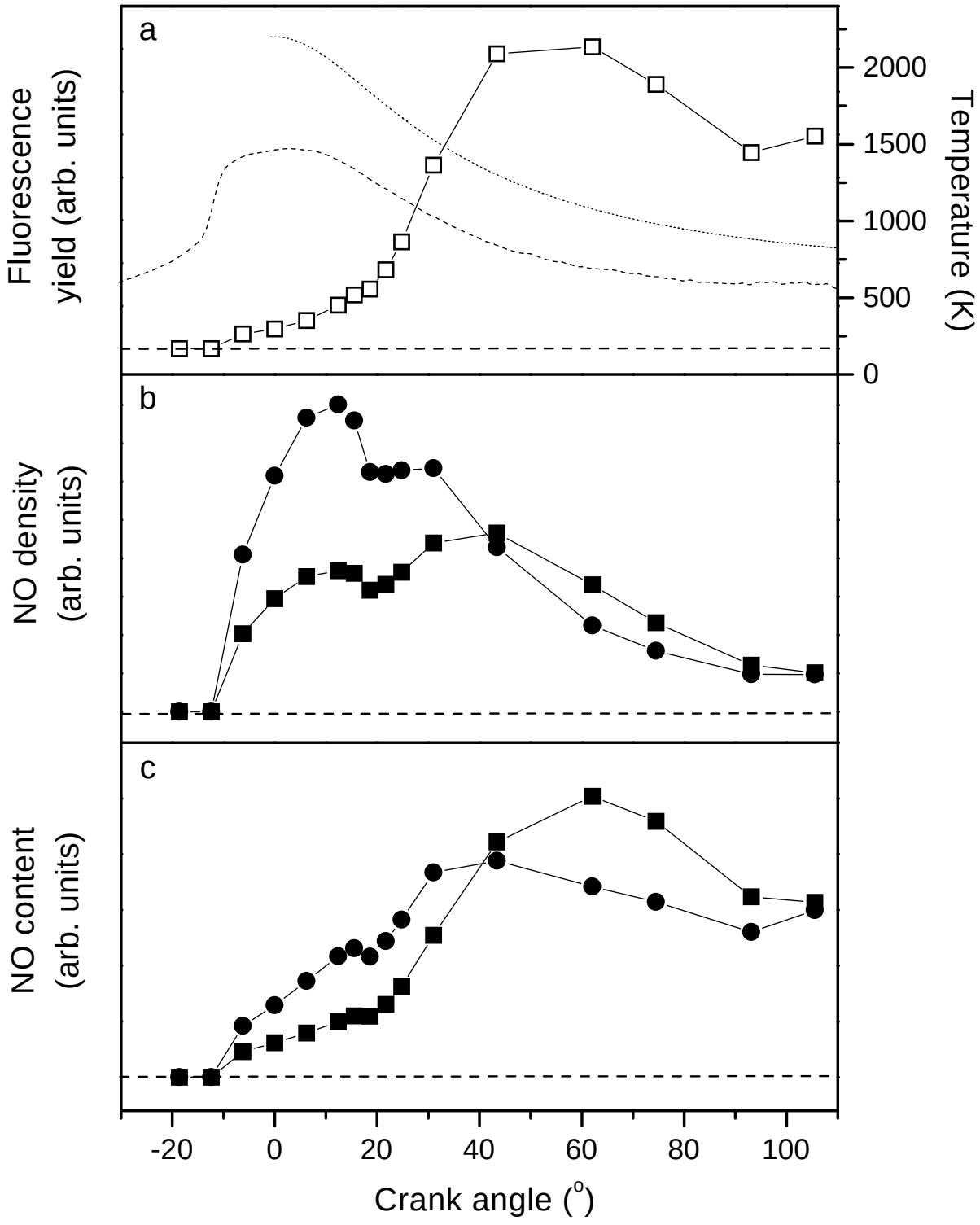

Figure 4: a) The integrated NO fluorescence yield obtained from the spectra given in figure 3 (open squares). The mean gas temperature (dashed line) and the soot temperature (dotted line) obtained at the same engine conditions are also included. b) Corresponding NO density following the procedures described in the Appendix, using either the mean gas temperature (solid black squares) or the soot temperature (solid circles). c) Corresponding NO content obtained by multiplying the curves in b) by the (crank angle dependent) cylinder volume. Engine running on fuel 1, $\epsilon = 14.4$ and 0.44 kW load.

the NO content is well established (equation 1 of the Appendix), some errors will be introduced by the assumptions made in obtaining the different factors that are used in the model. It is, for instance, not clear which temperature has to be used in the processing. Neither the soot temperature nor the mean gas temperature represents the local temperature at the position the NO is measured. During the actual combustion, the relevant temperature is probably higher than the mean gas temperature, as the cylinder contents are not likely to be in thermal equilibrium at that moment. The soot temperature may therefore be a better estimate for the NO temperature in the beginning of the combustion. However, this temperature will likely be too high at the end of the combustion, since the gases cool down faster than the soot particles. Probably, a realistic temperature of the probe volume is somewhere in between the two temperature curves of figure 4a. The effect of the two different temperatures is seen in figure 4b where NO density curves are given resulting from the same fluorescence yield curve using both temperatures. The use of the soot temperature results in a curve that shows a steeper rise of the NO density in the early phase of the combustion. (Note that both curves are in arbitrary units, so only their shapes should be compared.)

The NO density curve, given in figure 4b, shows that NO can first be detected at 6° bTDC and that its density increases throughout the combustion stroke till around 20° aTDC, depending slightly on the temperature used in the derivation. The subsequent decrease is largely due to the expanding in-cylinder volume, as can be seen from the NO content curves of figure 4c. The latter continue to rise up to about 50° aTDC, after which they more or less level off or show a small decrease. Comparison of the NO curves with the engine parameter curves of figure 2 leads to the conclusion that, in this (considerably modified) engine, the bulk of NO formation does not coincide with the highest pressure and temperature part of the stroke. Neither is any relation seen between the NO formation and the peak of the premixed burn in the heat release curve at 12° bTDC. At this crank angle only O_2 fluorescence is present in the spectra of figure 3, indicating that, although there definitely is laser intensity within the cylinder (and note that the O_2 fluorescence in all spectra up to 25° aTDC is about equally strong), the NO density is still below the detection limit. The bulk of NO formation takes place relatively late in the stroke, suggesting that the diffusion burning phase of combustion makes an important contribution to the NO formation.

The apparently late start of NO formation implied by the NO curves of figure 4 may raise the question whether all laser intensity might be absorbed early in the combustion chamber, before reaching the area where NO is formed. Although this possibility can not unequivocally be excluded (since the laser intensity cannot directly be measured within the cylinder), it is not considered very likely, again because of the presence of the O_2 fluorescence. This fluorescence originates from excitation of O_2 molecules in the $v''=2$ or 3 states. (In fact, the temperature dependence of the O_2 is even stronger than that of the NO fluorescence, because the lower levels involved are at a higher energy in O_2 ($v''=3$ $J''=5/15$ around 5800 cm^{-1}) than in NO ($v''=1$, $J''=26.5/32.5$ around 4300 cm^{-1})). Thus, it is likely that the O_2 fluorescence signal originates mainly in the highest temperature regions within the cylinder, that is, from around the spray edges where the premixed combustion occurs. This is also the region where NO might be expected to form (see images in Dec and Canaan [8]). Therefore, the absence of detectable NO fluorescence in the presence of hot O_2 fluorescence can be taken as an indication that NO formation has not yet begun at 12° bTDC.

This somewhat surprising result is supported by theoretical predictions by the group of Peters [18] and also by recent experimental results from other research groups [7, 8]. Nakagawa et al. [7] found that NO was formed on the lean side of the flame, where oxygen is present and the temperature is high. The region where NO is located was found to expand during the combustion, indicating that NO is not formed in the regions where the premixed combustion occurs. Images reported by Dec and Canaan [8] showed that, in their engine, NO formation starts around the jet periphery just after the diffusion flame forms. They found that NO remained confined to the edge of the jet until the jet structure disappeared. As the combustion continued, NO formation continued in the hot post-combustion gases, in the trail of the reacting fuel jet. Also, their NO content curve showed that NO formation does not arise from the premixed combustion but starts just after the diffusion flame forms and continues in the hot post-combustion gases after the end of the combustion. Only 67% of the NO had formed by the end of the apparent heat release. This is in contrast with models that predict that the premixed combustion has a large contribution to the NO formation and that NO_x emissions correlate with the amount of fuel consumed during the initial premixed burn [19, 20]. As several different laser diagnostic measurements are in agreement that the premixed burn is too fuel rich to produce significant NO, a correlation of NO_x emission with the fuel consumption during the premixed burn must arise for other reasons, as discussed in [8].

The small decline of the NO content curves at larger crank angles can possibly be explained by the fact that NO is not chemically stable. In the colder part of the stroke, NO can be oxidized to NO_2 (after the combustion there is still a lot of O_2 present), leading to a reduction of the NO content. This has also been predicted by calculations [18]. A relatively large conversion to NO_2 in this engine, used at a light load, would be consistent with a generally high NO_2/NO ratio at the exhaust occuring in light-load Diesel engines [16].

EFFECT OF ENGINE CONDITIONS

To study the effect of different engine conditions on the NO content, the compression ratio (ϵ), fuel and load were varied. Dispersed fluorescence spectra were recorded for the different engine conditions. They were evaluated using the mean gas temperature in the way described in the Appendix in order to obtain NO density curves as a function of crank angle. The NO density curves shown in figure 5a are obtained at different compression ratios

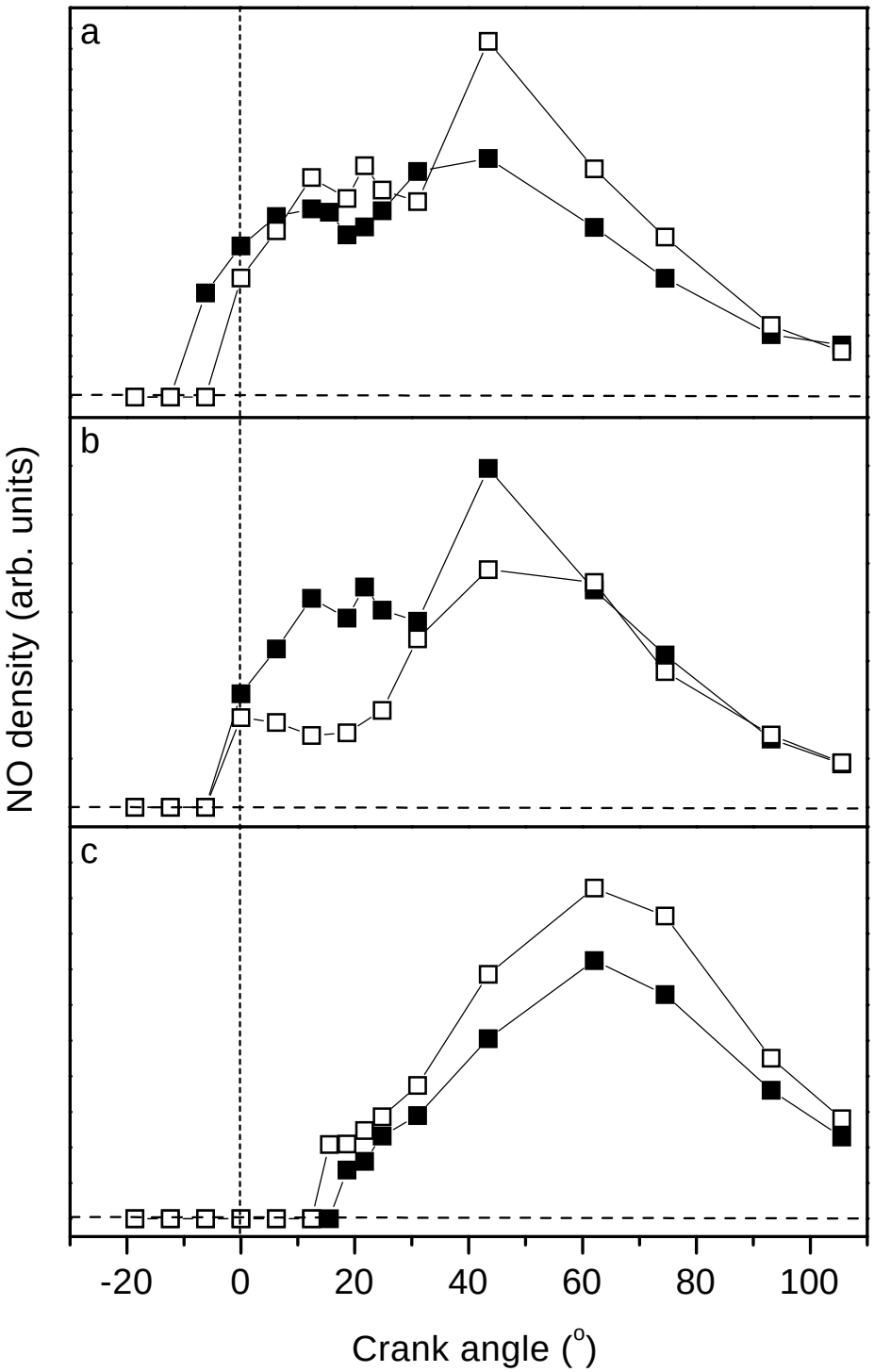

Figure 5: NO density curves obtained from the integrated NO fluorescence yield of dispersed fluorescence spectra recorded at different engine conditions.
a) Compression ratio ϵ=14.4 (solid black squares) and ϵ=13.4 (open squares); (fuel 1, 0.44 kW load)
b) Fuel 1 (solid black squares) and 2 (open squares); (ϵ=13.4, 0.44 kW load)
c) Load of 0.75 kW (solid black squares) and 0.88 kW (open squares); (ϵ=12.4, fuel 2)

(ϵ=14.4 (solid black squares); ϵ=13.4 (open squares)), those in figure 5b result from the engine running on different fuels (fuel 1 (solid black squares); fuel 2 (open squares)), and those in figure 5c are obtained from the engine loaded by different loads (0.75 kW (solid black squares); 0.88 kW (open squares)). From the curves in figure 5 it can be concluded that changing the engine conditions within these limits has only little influence on the NO content. A higher compression ratio leads to an earlier start of NO formation, as can be seen in figure 5a. This also follows from a comparison of the curves of figures 5a and c where the NO formation in the situation with the lower ϵ (figure 5c) starts much later. A possible explanation for this could be that, for lower compression ratios, the lower temperatures prevailing during most of the combustion cycle reduce all reaction rates, leading to a slower rise of the NO density to above the detection limit. (Note that absolute values in figure 5 may not be compared between graphs.) From figure 5b it follows that for both fuels NO formation starts at the same crank angle, but the early diffusion burning contributes more to the NO formation in the case of fuel 1. Because NO formation continues longer in the case of fuel 2, the densities reached at the end of the cycle are comparable. The influence of load can be derived from figure 5c. A higher load results in a slightly advanced rise of the NO density, which can be the result of the higher temperatures at higher loads, but otherwise the two curves are very similar.

As discussed in the context of figure 4, the density curves can be converted to NO content curves, thus removing the effect of the increasing in-cylinder volume. All NO content curves thus derived from figure 5 show a slow start of NO formation followed by a steep rise around 30° aTDC and a maximum around 80° aTDC, after which a small decrease follows. This indicates that, for all conditions studied, the NO formation does not arise from the initial premixed combustion but that the diffusion burning phase of combustion makes an important contribution.

CONCLUSION

The Laser Induced Fluorescence (LIF) technique was used to study the nitric oxide (NO) content and distribution inside the combustion chamber of an optically accessible two-stroke Diesel engine running on standard production Diesel. Using 193 nm excitation of NO and detection of the ensuing fluorescence at 216 nm allowed the determination of NO density throughout the whole combustion stroke.

Dispersed fluorescence spectra as a function of crank angle were measured. They show spectral structure resulting from NO fluorescence from 6° bTDC onwards. Close to TDC ($\Theta \lesssim 45°$ aTDC), additional fluorescence resulting from hot oxygen (O_2), partly overlapping the NO fluorescence bands, was seen. In the evaluation of the measured fluorescence signals, this interfering O_2 fluorescence was taken into account.

From the dispersed fluorescence spectra a relative measure for the amount of NO present inside the cylinder was obtained. In order to compare the amounts of NO throughout the stroke and for different engine conditions, fluorescence spectra were processed for the changing in-cylinder conditions (volume, pressure, temperature and laser radiation intensity). This transformation required knowledge of the local temperature within the probe volume.

The resulting NO content curves showed, for this engine, a slow start of NO formation followed by a steep rise around 30° aTDC to a maximum around 80° aTDC. This indicates that the diffusion burning phase of the combustion makes an important contribution to the NO formation and that NO formation continues in the hot post-combustion gases. This result is in agreement with the recently presented results from the group of Dec [8], showing that NO was formed at the periphery of the jet, starting just after the diffusion flame forms. Towards the end of the stroke a small decline of the NO content curves was seen. This could be due to the conversion of NO to NO_2 in the colder part of the stroke.

In the future, planar LIF will be used to obtain two-dimensional distributions of NO fluorescence, using the O_2 interference-free band at 208 nm. In addition, the LIF method will be applied on a realistic six-cylinder, direct-injection, 11.6 ℓ DAF Diesel engine. One of the cylinders is elongated and has been made optically accessible by a window in the piston and windows in the top of the cylinder wall. Also, other excitation/detection schemes will be pursued, notably using 226 nm excitation of NO in the $A(v' = 0) \leftarrow X(v'' = 0)$ band. First measurements using this excitation pathway are currently being evaluated [26].

ACKNOWLEDGEMENT

Many people have been involved in the initial preparations, modifications and maintenance of the two-stroke engine used in the measurements. In particular we would like to thank E. van Leeuwen, L. Gerritsen and P. van Dijk of the workshop of the University of Nijmegen for their enthusiastic and expert technical assistance, and P. Monkhouse for discussions on the interpretation of the fluorescence data. This research is supported by the Technology Foundation (STW) and the Netherlands' Organization for Applied Scientific Research (TNO).

References

[1] A.C. Eckbreth, "Laser diagnostics for combustion temperature and species", Abacus Press, Cambridge (1988).

[2] J.E. Dec, "Soot distribution in a DI Diesel engine using 2-D imaging of Laser-Induced Incandescence, Elastic Scattering, and Flame Luminosity", SAE paper no. 920115 (1992).

[3] C. Espey and J.E. Dec, "Diesel engine combustion studies in a newly designed optical-access engine us-

ing high-speed visualisation and 2-D laser imaging," SAE paper no. 930971 (1993).

[4] F. Hildenbrand, C. Schulz, V. Sick, G. Josefsson, I. Magnusson, Ö. Andersson and M. Aldén, "Laser spectroscopic investigation of flow fields and NO-formation in a realistic SI engine", SAE paper no. 980147 (1997).

[5] C. Schulz, V. Sick, J. Wolfrum, V. Drewes, M. Zahn and R. Maly, "Quantitative 2D single-shot imaging of NO concentrations and temperatures in a transparent SI engine", Proc. 26th Symp. (Int'l) on Combustion, 2597-2604, The Combustion Institute (1996).

[6] B. Alataş, J.A. Pinson, T.A. Litzinger and D.A. Santavicca, "A study of NO and soot evolution in a DI Diesel engine via planar imaging", SAE paper no. 930973 (1993).

[7] H. Nakagawa, H. Endo, Y. Deguchi, M. Matsuhei, H. Oikawa and T. Shimada, "NO measurements in Diesel spray flame using Laser Induced Fluorescence", SAE paper 970874 (1997).

[8] J.E. Dec and R.E. Canaan, "PLIF Imaging of NO Formation in a Diesel engine", SAE paper no. 980147 (1998).

[9] Th. Brugman, G.G.M. Stoffels, N. Dam, W.L. Meerts and J.J. ter Meulen, "Imaging and post-processing of laser-induced fluorescence from NO in a Diesel engine," Appl. Phys. B **64**, 717-724 (1997).

[10] M. Versluis, M. Ebben, M. Drabbels and J.J. ter Meulen, "Frequency calibration in the ArF laser tuning range using laser-induced fluorescence of NO", Appl. Opt. **30**, 5229-5234 (1991).

[11] P.H. Kruppenie, "The spectrum of molecular oxygen", J. Phys. Chem. Ref. Data. **1**, 423-534 (1972).

[12] A.M. Wodtke, L. Huwel, H. Schlüter, H. Voges. G. Meijer and P. Andresen, "Predissociation of O_2 in the B state", J. Chem. Phys. **89**, 1929-1935 (1988).

[13] M.P. Lee and R.K. Hanson, "Calculations of O_2 absorption and fluorescence at elevated temperatures for a broadband Argon-Fluoride laser source at 193 nm", J. Quant. Spectrosc. Radiat. Transfer. **36**, 425-440 (1986).

[14] M. Shimauchi, T. Miura and H. Takuma, "Absorption lines of vibrationally excited O_2 and HF in ArF laser spectrum", Jpn. J. Appl. Phys. **33**, 4628-4635 (1994).

[15] P. Flynn, M. Mizusawa, O.A. Uyehara and P.S. Myers, "An experimental determination of the instantaneous potential radiant heat transfer within an operating Diesel engine", SAE paper no. 720022 (1972).

[16] J.B. Heywood, "Internal Combustion Engine Fundamentals", McGraw-Hill, Singapore (1988).

[17] A. Bräumer, V. Sick, J. Wolfrum, V. Drewes, M. Zahn and R. Maly, "Quantitative two-dimensional measurements of nitric oxide and temperature distributions in a transparent square piston engine", SAE paper no. 952462 (1995).

[18] H. Pitsch, H. Barths and N. Peters, in A. Leipertz (ed.), "Berichte zur Energie- und Verfahrenstechnik", ESYTEC GmbH, Erlangen (Germany), **97.1**, 139-163 (1997).

[19] Ref. [16], p. 586-587.

[20] J. Warnatz, U. Maas and R.W. Dibble, "Combustion", Springer Verlag, Berlin (1996).

[21] K.P. Huber and G. Herzberg, "Molecular spectra and molecular structure IV. Constants of diatomic molecules", Van Nostrand Reinhold, New York (1979).

[22] A.A. Radzig and B.M. Smirnov, "Reference data on atoms, molecules and ions", Springer Verlag, Berlin (1985).

[23] R.W. Nicholls, "Approximate formulas for Frank-Condon factors", J. Chem. Phys. **74**, 6980-6981 (1981).

[24] M.C. Drake and J.W. Ratcliffe, "High temperature quenching cross sections for nitric oxide laser-induced fluorescence measurements", J. Chem. Phys. **98**, 3850-3865 (1992).

[25] P.H. Paul, J.A. Gray, J.L. Durant Jr. and J.W. Thoman Jr, "A model for temperature-dependent collisional quenching of NO $A^2\Sigma^+$", Appl. Phys. B **57**, 249-259 (1993).

[26] E.J. van den Boom *et al.*, in preparation.

[27] A.Y. Chang, M.D. DiRosa and R.K. Hanson, "Temperature dependence of collision broadening and shift in the NO A $\leftarrow$ X (0,0) band in the presence of argon and nitrogen", J. Quant. Spectrosc. Radiat. Transfer **47**, 375-390 (1992).

[28] M.P. Lee, B.K. McMillin and R.K. Hanson, "Temperature measurement in gases by use of planar laser-induced fluorescence imaging of NO", Appl. Opt. **32**, 5379-5396 (1993).

APPENDIX: SIGNAL PROCESSING

In order to quantify the measured fluorescence yield, all factors concerning the excitation of the molecules and the induced fluorescence resulting from the excited molecules have to be taken into account. For the case of pulsed excitation in which the fluorescence out of the excited state is recorded, the relation between the fluorescence signal measured by any given camera pixel, S_{LIF}, and the local NO density, ρ_{NO}, can be written as

$$S_{\mathrm{LIF}} = C \int_{\mathrm{V}} \rho_{\mathrm{NO}}(\vec{r}) I_{\mathrm{L}}(\vec{r}) A_{\mathrm{F}}(\vec{r}) f_{\mathrm{v,J}}(\mathrm{T}) \wp(\mathrm{P},\mathrm{T}) g(\nu_{\mathrm{L}},\nu_{\mathrm{a}}) \mathrm{d}^3 r \qquad (1)$$

where the integration is taken over the whole laser-illuminated volume seen by the detector. C is a proportionality constant, $I_{\mathrm{L}}(\vec{r})$ is the local intensity of the laser beam and $A_{\mathrm{F}}(\vec{r})$ is a factor describing the attenuation of induced fluorescence on its way to the top window. The Boltzmann fraction, $f_{\mathrm{v,J}}(\mathrm{T})$, describes the temperature dependent population of the probed state. The Stern-Vollmer factor, $\wp$(P,T), accounts for the competition between radiative and non-radiative (collision-induced) decay of excited molecules, and $g(\nu_{\mathrm{L}},\nu_{\mathrm{a}})$ is the overlap integral of the laser line profile with the NO absorption spectrum. In the model rotational energy transfer in the ground state is neglected because of the low laser intensity inside the engine.

In order to extract a NO density from the measured fluorescence yield, all factors in equation 1 have to be known. However, although the general relationship between the fluorescence yield and the NO content is clear, most of the individual factors are difficult to obtain. Furthermore, evaluation of these factors results in expressions which depend on the in-cylinder conditions (volume, pressure, temperature and laser intensity) of which particularly the temperature is insufficiently known. The evaluation of the individual factors of equation 1 is discussed below for the case of laser illumination and fluorescence detection both through the top window.

Ideally, each (square) CCD pixel collects fluorescence from a square rod parallel to the cylinder axis and extending from the bottom of the top window downwards (z-direction; z=0 at the top window). In practice, some averaging will take place due to the finite depth of field of the camera objective (f/4.5), as well as some image blurring due to the slightly etched lower surface of the observation window. Neglecting these effects for the present analysis, and taking into account that the spectra in figure 3 represent averages over the slit height, equation 1 can be rewritten as

$$\begin{aligned} S_{\mathrm{LIF}}(\lambda) &= C(\lambda) \int_{z=0}^{z_p} \rho_{\mathrm{NO}}(z) I_{\mathrm{L}}(z) A_{\mathrm{F}}(z) f_{\mathrm{v,J}}(\mathrm{T}) \wp(\mathrm{P},\mathrm{T},\lambda) g(\nu_{\mathrm{L}},\nu_{\mathrm{a}},z) \mathrm{d}z \\ &\approx C(\lambda) \overline{\rho}_{\mathrm{NO}} f_{\mathrm{v,J}}(\overline{\mathrm{T}}) \overline{\wp(\mathrm{P},\overline{\mathrm{T}},\lambda)}\, \overline{g(\nu_{\mathrm{L}},\nu_{\mathrm{a}})} \int_{z=0}^{z_p} I_{\mathrm{L}}(z) A_{\mathrm{F}}(z) \mathrm{d}z \end{aligned} \qquad (2)$$

in which z_p is the position of the piston upper surface. In the second step several proportionality factors have been replaced by their average values over the measured volume (indicated by overbars), which allows to take them out of the integral. This model, therefore, provides a value for the *average* NO density in the whole volume seen by the detector (the probe volume).

Proportionality constant C: This factor is just a gauge constant including a number of experimental parameters like collection efficiency, window transmission, camera sensitivity, etc. This factor is constant during the whole combustion stroke.

Local laser intensity $I_{\mathrm{L}}(z)$ **and Fluorescence attenuation** $A_{\mathrm{F}}(z)$: On its way through the combustion chamber both the laser radiation and the induced fluorescence suffer attenuation, due mainly to absorption by and scattering off soot particles and fuel and oil droplets. The intensity of the laser beam, with an intensity I_0 when it enters the combustion chamber, can be written as

$$I_{\mathrm{L}}(z) = I_0 \exp(-\int_0^z \alpha(z')\rho_{\mathrm{s}}(z')\mathrm{d}z'), \qquad (3)$$

in which α is an effective extinction cross section and ρ_{s} is the density of the attenuating particles. A similar equation holds for the fluorescence attenuation, $A_{\mathrm{F}}(z)$. In general, both α and ρ_s will be a function of position z. The local extinction coefficient is an inaccessible parameter, that cannot be measured. An approximation can be made by replacing $\alpha(z)\rho_s(z)$ by its average, $\overline{\alpha\rho_s}$. In this approximation, and combining the equations for I_{L} and A_{F}, the integral in equation 2 can be written as

$$\begin{aligned} \int_{z=0}^{z_p} I_{\mathrm{L}}(z) A_{\mathrm{F}}(z) \mathrm{d}z &\approx I_0 \int_{z=0}^{z_p} \exp(-2\overline{\alpha\rho_s} z') \mathrm{d}z' \\ &= \frac{\delta I_0}{2} (1 - \exp(-2z_p/\delta)) , \end{aligned} \qquad (4)$$

in which a penetration depth δ has been defined as $\delta = 1/\overline{\alpha\rho_s}$. Also, $\overline{\alpha\rho_{\mathrm{s}}}$ has been assumed to be the same at the wavelengths of excitation (193 nm) and fluorescence detection (216 nm in the case of figure 3).

A measure for the average extinction coefficient over the whole cylinder can be obtained from transmission

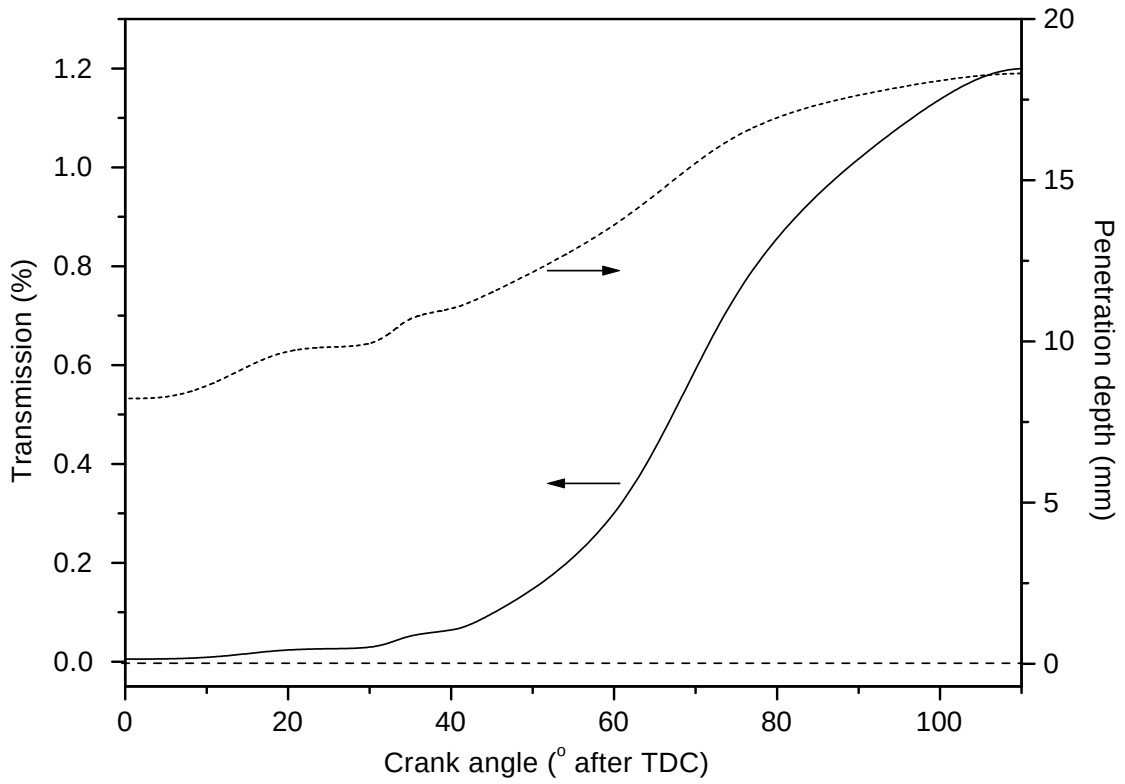

Figure 6: Transmission of the laser beam (solid line; λ=193.377 nm) through the firing engine (based on 10% window transmission). It is measured by coupling the laser beam in and out through the side windows and detecting the transmitted radiation behind the outcoupling window. Also included is the penetration depth defined in equation 4 (dashed line).

measurements of the laser beam, employing the side windows (figure 1; W1,2). These data, given in figure 6, show a rise in transmission around 60° aTDC, which coincides with the end of the visible combustion, suggesting that unburned fuel plays a part in the absorption of 193 nm laser radiation. Apart from this, the expansion also reduces the density of soot and other absorbing species, which causes less attenuation of the laser radiation with increasing crank angle. The penetration depth of the laser radiation, defined in equation 4, is also included in figure 6. Evidently, the setup is most sensitive for fluorescence signals originating in the uppermost part of the cylinder, even when the piston has moved to BDC.

For the interpretation of the spectra of figure 3, we have assumed the *average* extinction coefficient obtained from the transmission measurements to be equal to the *average* extinction coefficient $\overline{\alpha\rho_s}$ of equation 4. It has, however, been checked that changing these values by as much as a factor of 10 (both smaller and larger) has relatively little influence on the *shape* of the NO density curves as a function of crank angle (the absolute numbers do change, of course, but these are arbitrary units anyway).

Boltzmann fraction $f_{\mathrm{v,J}}(\overline{\mathrm{T}})$: The temperature dependent fractional population of the probed state ($\mathrm{v''}$=1, J=26.5/32.5) can be calculated using the well established spectroscopic data of the NO electronic ground state [21]. For the average temperature $\overline{\mathrm{T}}$ either the mean gas temperature or the soot temperature has been used.

Stern-Vollmer factor $\wp(\mathrm{P},\overline{\mathrm{T}})$: The competition between the radiative and non-radiative decay channels is described by the Stern-Vollmer factor,

$$\wp(\mathrm{P},\overline{\mathrm{T}},\lambda) = \frac{\mathrm{A_{v'v''}}}{\sum\limits_{v''}\mathrm{A_{v'v''}} + \mathrm{Q}} \approx \frac{\mathrm{A_{v'v''}}}{\mathrm{Q}}. \qquad (5)$$

The radiative decay rate, $\mathrm{A_{v'v''}}$, can be estimated from the radiative lifetime of the D-state (τ=18 ns [22]) and the Frank-Condon factor for the used fluorescence transition D($\mathrm{v'}$=0) $\rightarrow$ X($\mathrm{v''}$=4) at 216 nm (0.076, calculated using a model of Nicholls [23] and the spectroscopic data of NO [21]). The non-radiative decay rate, Q, is caused by intermolecular collisions including both EET (D $\rightarrow$ C and D $\rightarrow$ A) and quenching (D $\rightarrow$ X). For the A state, data on quenching are available in literature [24, 25], but little is known for the D state. Separate measurements in a high temperature, high pressure cell have shown that D $\rightarrow$ A electronic energy transfer induced by collisions with N_2 is a very effective decay channel [26]. Since N_2 is always the major species in the combustion chamber, it is assumed for the moment that the non-radiative decay rate of the D($\mathrm{v'}$=0) level in the engine is dominated by N_2 collision-induced EET to the A-state, so that the detailed composition of the burning mixture is relatively

unimportant. (Note that N_2 is an inefficient quencher of the A(v′=0) level (see e.g. ref. [24]), but that EET plays no role in the non-radiative decay of the lowest excited electronic state.) Therefore, Q can be written as $Q = \overline{v}\rho_c\sigma$, in which $\overline{v} = \sqrt{8k\overline{T}/\pi\mu}$ is the mean relative velocity of the collision partners at a total density ρ_c ($\propto P/\overline{T}$) and σ is an effective quenching cross section, taken to be independent of pressure and temperature. In the firing engine $Q \gg A$ [1, 26] and therefore $\wp(P,\overline{T}) \propto \sqrt{\overline{T}}/P$.

Overlap integral $g(\nu_L,\nu_a)$: The overlap integral is calculated by assuming Gaussian profiles for both the laser emission ($L(\nu-\nu_L)$) and the NO absorption line ($N(\nu-\nu_a)$), with central frequencies ν_L and ν_a, respectively. A shift in the position of the lines is not taken into account because the laser is tuned to resonance ($\nu_L = \nu_a$), under engine conditions, before each measurement. This results in:

$$g(\nu_L,\nu_a) = \int_{-\infty}^{+\infty} L(\nu-\nu_L)N(\nu-\nu_a)d\nu \;\propto\; \frac{1}{\sqrt{\Delta_L^2+\Delta_a^2}}\,, \tag{6}$$

in which Δ_L and Δ_a are the widths (FWHM) of the laser emission line and the NO absorption line, respectively. Δ_L is constant (1 cm^{-1}) but Δ_a is affected by the changing pressure and temperature during the stroke. Calculation of Δ_a requires information about the pressure broadening of the NO absorption lines in the D(v′=0) ← X(v″=1) band under engine conditions. These data are not available in literature. For the present purpose the functional pressure and temperature dependence of the A ← X band is taken [27, 28], in combination with a proportionality factor that is derived from own measurements on the D ← X band in the engine, yielding

$$\Delta_a = 0.53\,P\left(\frac{295}{\overline{T}}\right)^{0.75} cm^{-1}, \tag{7}$$

with P the pressure in bar and $\overline{T}$ the average temperature in Kelvin.

Following the procedure described above, relative values for the average NO density within the probe volume can be extracted from the fluorescence yield as a function of crank angle. To the extent that the probe volume is representative for the whole cylinder (which seems not unreasonable, in view of the illuminated area indicated in figure 1 and the penetration depth of figure 6), these density data can be related to an in-cylinder NO content by multiplication with the (crank angle dependent) in-cylinder volume,

$$N_{NO} \propto \overline{\rho_{NO}}\,V(z_p)\,. \tag{8}$$